IEEE Access
Multidisciplinary ⋮ Rapid Review ⋮ Open Access Journal

Received 10 May 2024, accepted 27 May 2024, date of publication 3 June 2024, date of current version 10 June 2024.

Digital Object Identifier 10.1109/ACCESS.2024.3408920

RESEARCH ARTICLE

Dual-Band Dual-LP/CP Antennas Using Combined Metasurface and Patch For UHF/2.45-GHz RFID Readers

THI NGOC HIEN DOAN, KHAC KIEM NGUYEN, (Member, IEEE), AND SON XUAT TA, (Senior Member, IEEE)

School of Electrical and Electronic Engineering, Hanoi University of Science and Technology, Hanoi 100000, Vietnam

Corresponding author: Son Xuat Ta (xuat.tason@hust.edu.vn)

This research is funded by Hanoi University of Science and Technology (HUST) under project number T2023-TD-005.

ABSTRACT This paper proposes dual-band dual linearly-polarized (LP)/circularly-polarized (CP) antennas using combined metasurface and patch for ultra high frequency (UHF) and 2.45-GHz RF identification (RFID) readers. A metasurface and two stacked patches are employed for the lower and upper bands, respectively. The metasurface and patches are incorporated with a common feeding structure which is composed of two orthogonal microstrip lines and a crossed slot to produce the dual-wideband dual-LP radiation. To reduce the back radiation and improve the gain, the antenna is backed by a metallic cavity. Taking advantage of its low-profile structure, the dual-LP antenna is further integrated with a dual-band branch-line coupler to realize dual-CP radiation. Both proposed antennas yield stable radiation performances across dual operating bands which completely cover the assigned RFID spectrum at the UHF (860 − 960 MHz) and 2.45-GHz (2400 − 2500 MHz) bands.

INDEX TERMS Dual-band, dual polarization, metasurface, patch antenna, RF identification (RFID), backed-cavity, hybrid coupler, multiple-input multiple-output.

I. INTRODUCTION

Radio frequency identification (RFID) is a type of automatic-identification/data-collection technology that utilizes electromagnetic (EM) waves to identify any object integrating with electronic tag (also named RFID tag) [1]. Thanks to advantages of low-cost, fast reading speed, agility, and endurance, the RFID has been widely applied to public transportation, manufacturing companies, logistics, and so on [2]. The RFID system is generally composed of a host computer connected to networks, readers, and tags. The reader transmits a continuous EM wave to activate the tag. Once powered up, the tag receives commands from the reader and answers by switching the load of its antenna. According to the communication distance between the reader and tag, the RFID is divided into near-field and far-field systems [1]. Frequency bands of 125−135 kHz and 13.5 MHz are assigned for the near-field RFID systems, while ultrahigh frequency (UHF) 433.92/860−960 MHz and industrial scientific and medical (ISM) 2.45/5.8 GHz bands are assigned for the far-field RFID systems. In the recent years, the far-field RFID system has been receiving much attention due to its features of lower cost, higher data rate, faster reading/writing speed, and longer communication range. Among with these attentions, there have been higher demands raised in designing antennas for far-field RFID readers.

Different UHF RFID bands are assigned in different countries. For the universal applications, reader antennas are designed to fully cover the UHF RFID band of 860−960 MHz [3]. Since the tag are normally linearly polarized (LP), circularly polarized (CP) antennas have been preferred for the readers [4], [5], [6], [7], [8]. Several techniques have been presented for a wideband CP radiation, which, for instant, include stacked patches [4], corner truncated patch loaded with slits and modified

The associate editor coordinating the review of this manuscript and approving it for publication was Li Yang.

ground plane [5], [6], circular slot antenna with L-shaped strips [7], and sequentially rotated array [8]. Moreover, for a higher range and a high data transfer rate, integration UHF (860−960 MHz) and 2.45-GHz bands into one RFID system has been implemented for various applications. Therefore, several dual-band antennas have been proposed for the UHF/ISM 2.45-GHz RFID readers. For handheld applications, simple structure, compact size, light weight, and easy realization are required in the designed antennas [9], [10], [11], [12]. For other applications with non-restricted area for readers, the antennas are designed for dual wideband, CP radiation, and high gain [13], [14], [15], [16], [17]. These dual-band antennas, however, are with single input port only.

To increase the reliability of data transmission, using RFID multiple-input multiple-output (MIMO) systems has been investigated mainly through simulations and measurements [18], [19], [20]. A typical RFID MIMO system requires multi-port Tx/Rx one-body antenna for its reader. So far, research papers reporting antennas for the RFID MIMO readers are rare. In [21], a patch is fed by a branch-line coupler through H-shaped slots to provide a dual-CP radiation at 860−940 MHz. For a dual-band dual-sense radiation at the UHF/ISM RFID bands, a rectangular patch is incorporated with a dual-band metamaterial branch-line coupler [22]. This design, however, suffers a narrow bandwidth for 10-dB port-to-port isolation.

This paper proposes dual-band dual-LP/CP antennas using combined metasurface and patch for UHF/ISM 2.45-GHz RFID readers. The proposed design employs metasurface resonance and fundamental mode of two stacked patches for the lower and upper bands, respectively. The primary radiating elements are fed by a common feeding structure that consists of two orthogonal microstrip lines and a crossed slot to produce the dual-wideband dual-LP radiation. To mitigate the back radiation and improve the gain, the crossed slot is shielded by a metallic cavity. For generating a broadside dual-CP radiation, the dual-LP antenna is integrated with a dual-band branch-line coupler. The performances of the proposed designs are computationally demonstrated by using ANSYS Electronics Desktop and confirmed by measurements.

II. DUAL-BAND DUAL-LP ANTENNA

A. GEOMETRY

Fig. 1 shows the geometry of dual-band dual-LP antenna. It is composed of a metasurface, two stacked patches (Patch 1 and 2), a ground plane (GND), a metallic cavity, a feeding structure, and three substrates (Subs. 1−3). The GND is placed on the bottom side of Sub. 1 (Roger RO4003, $\varepsilon_r = 3.38$, $\tan\delta = 0.0027$, and thickness of 0.8128 mm). The feeding structure inspired by [23] consists of two orthogonal microstrip lines (printed on the top side of Sub. 1) and a crossed slot (etched on GND). Each feed line consists of a 50−Ω line, a T-junction power divider, and two 100−Ω lines. Each microstrip line is coupled with a linear slot for either vertically- or horizontally-polarized radiation. Accordingly,

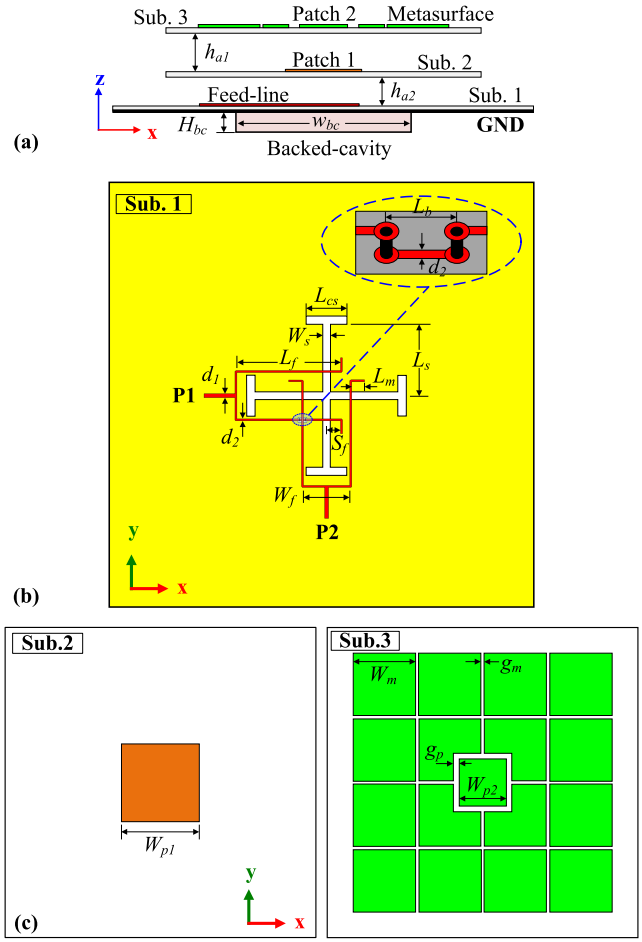

FIGURE 1. Geometry of the dual-band dual-LP antenna using combined metasurface and patch: (a) cross-sectional view, (b) top view of Sub. 1, (c) top view of Subs. 2 and 3. Its design parameters are as: $d_1 = 1.9$, $d_2 = 0.8$, $L_f = 57.2$, $W_f = 23$, $S_f = 8$, $L_m = 6.2$, $L_s = 37.5$, $W_s = 4$, $L_{cs} = 19.8$, $L_b = 4$, $W_{p1} = 45$, $W_{p2} = 26.5$, $W_m = 36$, $g_m = 0.2$, $g_p = 1.75$, $h_{a1} = 14$, $h_{a2} = 8$, $H_{bc} = 10$, $w_{bc} = 110$ (units in mm).

the two orthogonal microstrip lines are coupled with the crossed slot to generate the dual polarization. To avoid overlap between the feedlines, a bridge is inserted into a microstrip line to establish a crossover, as illustrated inset of Fig. 1(b). The crossed slot is backed by the metallic cavity to mitigate the back radiation, but remain a low profile [24]. The Patch 1 is placed on the top side of Sub. 2 (FR4, $\varepsilon_r = 4.4$, $\tan\delta = 0.02$, and thickness of 1 mm), while the metasurface and Patch 2 are built on the top side of Sub. 3 (FR4, $\varepsilon_r = 4.4$, $\tan\delta = 0.02$, and thickness of 1 mm). The three substrates are separated by two air gaps of h_{a1} and h_{a2}, respectively. The antenna is characterized by using ANSYS Electronics Desktop to achieve a dual-LP radiation at 0.9 and 2.45 GHz. Its optimized parameters are listed in the caption of Fig. 1.

B. METASURFACE RESONANCE

Metasurfaces, which are 2-dimension planar arrays of uniform or nonuniform sub-wavelength metallic or dielectric

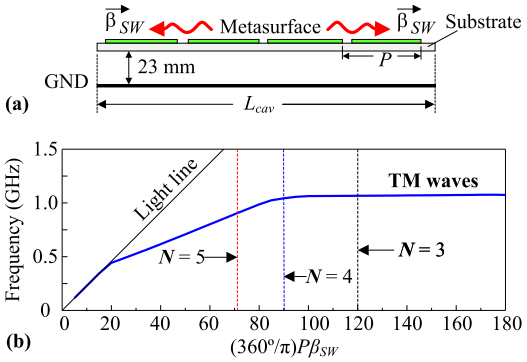

FIGURE 2. (a) Surface waves propagating on the metasurface-based antenna; (b) dipersion diagram of the metasurface and graphical solution of equation (1) for different numbers of cells.

TABLE 1. Surface-wave resonances of the antenna using metasurface for different numbers of cells.

Metasurface sizes	3 × 3 cells	4 × 4 cells	5 × 5 cells
f_{SW} obtained by cavity model	1.05 GHz	1.02 GHz	0.92 GHz
f_{SW} obtained by the full-wave simulation	1.1 GHz	1.01 GHz	0.95 GHz

atoms, can be used as primary radiating elements in designing antennas [25]. Broadband characteristics of a metasurface with a low-profile structure have been exploited in the metasurface-based antennas, e.g., [26], [27], [28]. The metasurface with finite size have been properly designed to generated resonances for the antenna systems. At these resonances, the metasurface size equals the resonance length of given surface waves propagating on the metasurface panel [26], as illustrated in Fig. 2(a). Using the cavity model [27], the surface wave resonances can be obtained as:

$$\beta_{SW} = \frac{\pi}{L_{cav}} = \frac{\pi}{N \times P} \tag{1}$$

where β_{SW} is the propagation constant of the certain wave at the resonance, L_{cav} is the length of metasurface panel, N is the number of cells, and P is the periodicity of the metasurface structure.

To predict the metasurface resonances of the proposed antenna, the equation (1) is computationally solved by using Eigenmode of the ANSYS Electronics Desktop. The dispersion diagram of the metasurface structure is calculated with linked boundary conditions in the full-wave simulator. The first eigenmode (TM waves) is calculated and illustrated in Fig. 2(b). The surface-wave resonances are intersections between vertical lines for $N = 3, 4, 5$ and the dispersion curve, which are listed in Table 1. It is observed that as the number of cells increased, the surface wave resonance shift toward the lower frequency.

In order to confirm the results obtained by the cavity model, a metasurafce-based antenna [as shown in Fig. 3(a)] is computationally characterized by using the ANSYS

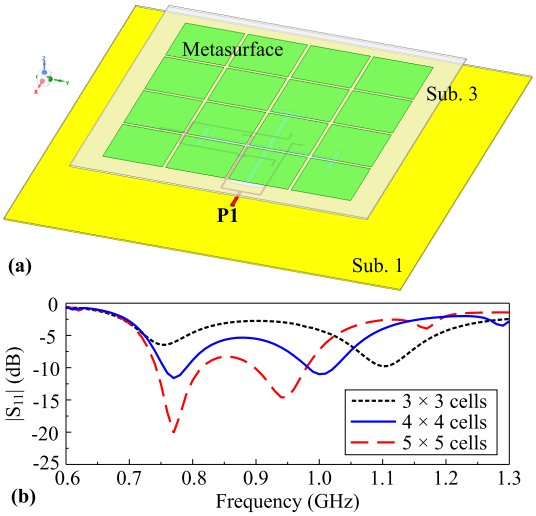

FIGURE 3. (a) Geometry of metasurface-based antenna with slotted feed; (b) its simulated $|S_{11}|$ values for different numbers of cells (N).

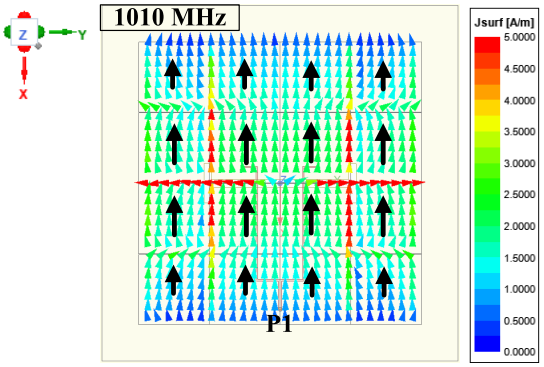

FIGURE 4. Simulated current distributions on the antenna configuration with 4 × 4-cell metasurface at its resonances when P1 is excited.

Electronics Desktop for different numbers of cells and the simulated $|S_{11}|$ values are shown in Fig. 3(b). All design parameters of the metasurface-based antenna are the same as those of the proposed design given in Fig. 1. From Fig. 3(b), the antenna yields two resonances in the $|S_{11}|$ curves. As N increased, the lower resonance hardly changed, whereas the upper one shifted toward the lower frequency. It can conclude that the lower resonance is caused by the slot feed, while the upper resonance is generated by the metasurface. The metasurface resonances obtained by the full-wave simulator are also summarized in Table 1 and compared to the cavity model. The results agreed rather closely and indicate that metasurface resonances are mainly determined by the number of cells.

For a further investigation, current distribution on the antenna configuration with 4 × 4-cell metasurface is calculated at 1010 MHz and given in Fig. 4. The current distribution confirms that the metasurface mode is TM_{10}. Also, it is observed that all currents are in-phase, which indicates a good broadside radiation.

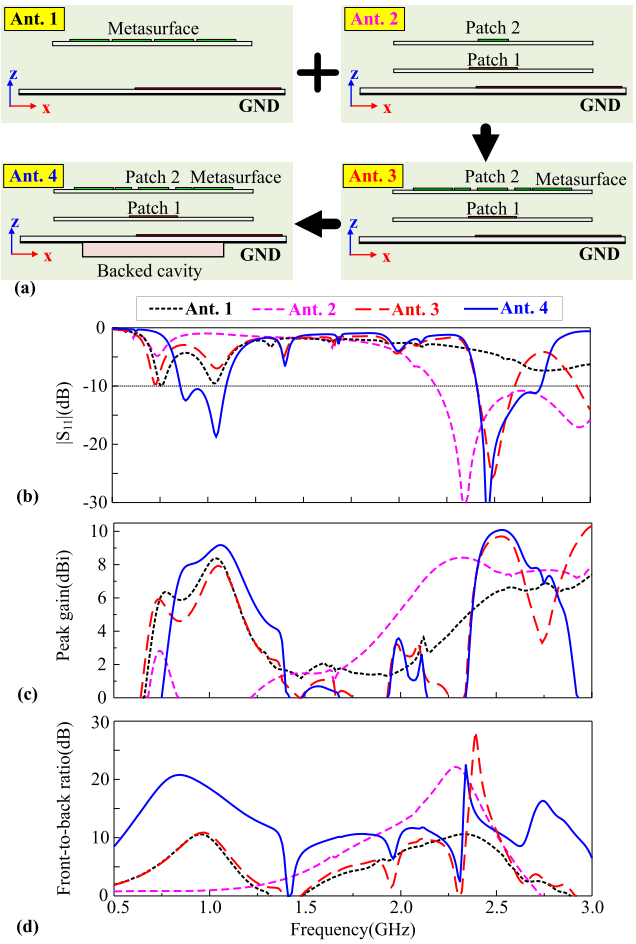

FIGURE 5. (a) Design evolution of the dual-band dual-LP antenna; simulated (b) $|S_{11}|$, (c) peak realized gain, and (d) front-to-back ratio for different steps.

C. DESIGN EVOLUTION

The proposed dual-band dual-LP antenna is implemented based on a combination of metasurface and stacked patches. To illustrate the radiation mechanism, Fig. 5(a) shows its design evolution. The metasurface-based antenna with 4×4-cells (Ant. 1) is selected for 0.9-GHz band, while a stacked patch antenna (Ant. 2) is selected for 2.45-GHz band. Ant. 3 is a combination of metasurface and patch design to obtain dual-band operation at 0.9 and 2.45 GHz. A backed-cavity is added to Ant. 3 to create the proposed antenna (Ant. 4). For demonstration, the design parameters of all configurations are the same as those of the proposed design, which are listed in the caption of Fig. 1. All antennas are characterized and their results are given in Figs. 5(b-d).

From Fig. 5(b), Ant. 1 yields a single band at 0.9 GHz, while Ant. 2 exhibits an operational band at 2.45 GHz. On the other hand, Ant. 1 has a resonance around 2.75 GHz which could be caused by a higher order mode of the metasurface; Ant. 2 has a resonance around 0.75 GHz which is observably caused by the cross-slot feed. Ant. 3 is the combination of metasurface and stacked patches, and therefore, which achieves a dual-band operation at 0.9 and 2.45 GHz. Since

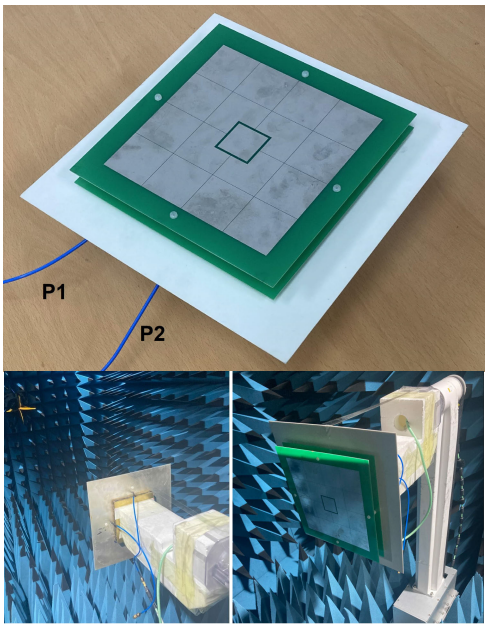

FIGURE 6. A fabricated prototype of the dual-band dual-LP antenna (inset: setup for far-field measurements).

the Ants. 1 – 3 employ the aperture coupled feed, they suffer a drawback of large back radiation, as illustrated in Figs. 5(c, d). Ants. 1 – 3 yield low values in terms of gain and front-to-back ratio, especially, in the lower band. To address this problem and remain the low profile, the proposed antenna (Ant. 4) employs a backed cavity [24]. The metallic cavity is electrically grounded and presents the EM waves radiated from the crossed slot, and consequently, it makes the antenna stable and reproducible. As shown in Fig. 5(b), the presence of cavity shifts the slot resonance toward the higher frequency, and consequently, Ant. 4 achieves a 10-dB return loss bandwidth of 0.85–1.09 GHz and 2.4–2.74 GHz. With the cavity, Ant. 4 achieves significantly higher gain and front-to-back ratio as compared to other configurations, as illustrated in Figs. 5(c, d).

D. FABRICATION AND MEASUREMENT

The final design of dual-band dual-LP antenna has been fabricated and measured. Fig. 6 shows photographs of the antenna prototype with overall size of $24 \times 24 \times 3.4$ cm^3 ($0.72\lambda \times 0.72\lambda \times 0.1\lambda$ at 0.9 GHz). The feeding structure, metasurface, and stacked patches are realized using the standard printed circuit board technology, while the cavity is made from 0.2-mm copper plates. The components are fasten together by using plastic posts and screw.

Fig. 7 illustrates simulated and measured S-parameters of the dual-band dual-LP antenna prototype. The simulation agrees rather closely with the measurement and both indicate that the antenna achieves a dual-band operation and high port-to-port isolation. The measurements result in an impedance matching bandwidth of 0.86–1.08 GHz and 2.40–2.75 GHz and an isolation of $\geq$ 30 and 25 dB for the lower and

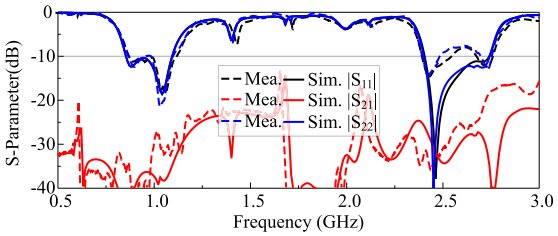

FIGURE 7. Simulated and measured S-parameters of the dual-band dual-LP antenna prototype.

upper bands, respectively. A minor breach occurs in the measured reflection coefficients at about 2.6 GHz (about −8 dB). This breach could be attributed to the realization tolerances.

Figs. 8 and 9 show the normalized radiation pattern of the antenna prototype when the P1 and P2 are excited, respectively. Again, there is a good agreement between the simulation and measurement. For both bands, the antenna yields a good dual-polarized radiation with highly symmetric pattern, low cross-polarization level, and high front-to-back ratio. At the lower band, for both ports, the measurements result in a cross-polarization level of < -25 dB, a front-to-back ratio of > 20 dB, and half-power beamwidths (HPBWs) of $70° \pm 5°$ in the $E-$ and $H-$planes. At 2.45 GHz, the E-plane pattern is split into three slobes, which is attributed to a side effect of the combination of metasurface and stacked patch; i.e., there is a higher-order mode resonance of the metasurface appeared at the upper band [see $|S_{11}|$ curve of Ant. 1 in Fig. 5(b)]. The split-beam pattern results in a broad beamwidth which could provide a broad coverage for the RFID reader. Nevertheless, within the upper band, the measurements result in a cross-polarization level of < -25 dB and a front-to-back ratio of > 15 dB.

Fig. 10 illustrates the peak realized gains of the dual-band dual-LP antenna prototype. The measurements result in the peak gains of 10.0 and 9.3 dBi at the lower and upper bands, respectively, which are relative to the simulated values of 9.2 and 10.1 dBi. Due to the function limitation of the anechoic chamber, the radiation efficiencies (REs) have not been measured. Nevertheless, the simulations result in the peak RE values of 94% and 84% at the lower and upper bands, respectively.

III. DUAL-BAND DUAL-CP ANTENNA

A. SCHEMATIC MODEL AND ANTENNA GEOMETRY

As mentioned above, besides the dual-band operation in one structure, CP radiation is also an important aspect of the RFID reader antenna; i.e., the CP antenna allows RFID readers to communicate LP tags regardless of arrangement and polarization-loss reduction, and therefore, which provide more communication reliability between readers and tags. As shown in Fig. 11, the traditional method for generating dual-CP waves is an incorporation of a LP antenna and a 90° hybrid coupler [29]. Extending this method, a dual-band dual-CP antenna is established by combining a dual-band 90°

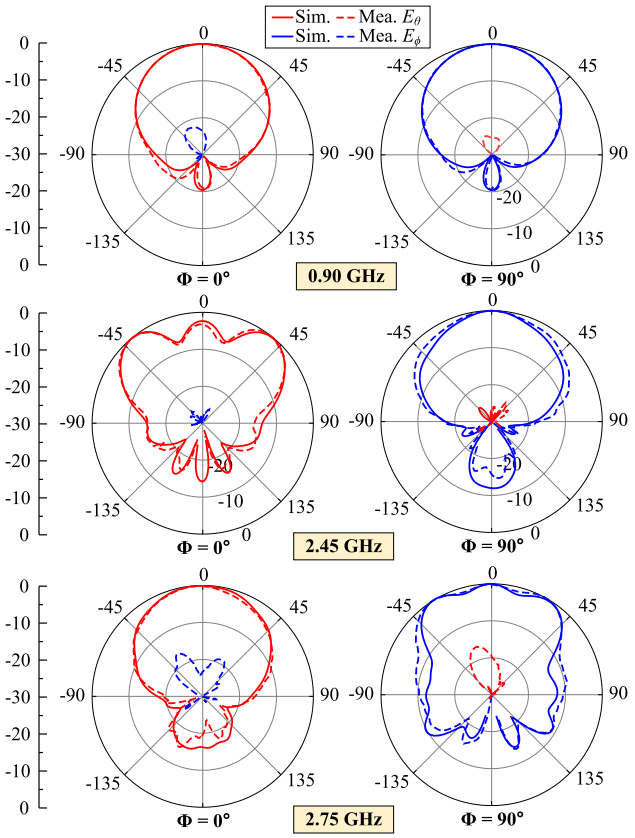

FIGURE 8. Normalized radiation pattern of the dual-band dual-LP antenna prototype when P1 is excited.

hybrid coupler and dual-band dual-LP radiator presented in the previous section. Key considerations for this combination are as follows:

1) The operational bandwidth of the coupler should cover the bandwidth of the dual-band dual-LP antenna.
2) The implementation of the coupler does not increase the complexity and overall size of the antenna.

The geometry of the dual-band dual-CP antenna is illustrated in Fig. 12. Its primary radiating elements are similar to the dual-band dual-LP antenna. Its feeding network is a two-stage coupler with open stubs, which is printed on the top side of Sub. 1. The antenna is optimized for the dual-band dual-CP radiation at 0.9 and 2.45 GHz bands. Referring to Figs. 1 and 12, its optimized design parameters are as: $d_1 = 1.9$, $d_2 = 0.8$, $L_f = 51.2$, $W_f = 30$, $S_f = 7$, $L_m = 7.2$, $L_s = 35$, $W_s = 4$, $L_{cs} = 19$, $L_b = 3$, $W_{p1} = 45$, $W_{p2} = 26.5$, $W_m = 36$, $g_m = 0.2$, $g_p = 1.75$, $h_{a1} = 14$, $h_{a2} = 8$, $H_{bc} = 10$, $w_{bc} = 100$ (unit: mm).

B. DUAL-BAND HYBRID COUPLER

In the proposed dual-band dual-CP antenna, the dual-band 90° coupler is inspired by [30], as shown in Fig. 13. The feeding structure consists of two-section branch-line coupler and eight stepped-impedance stubs, which is compensated for the Roger RO4003 substrate ($\varepsilon_r = 3.38$, $\tan\delta = 0.0027$,

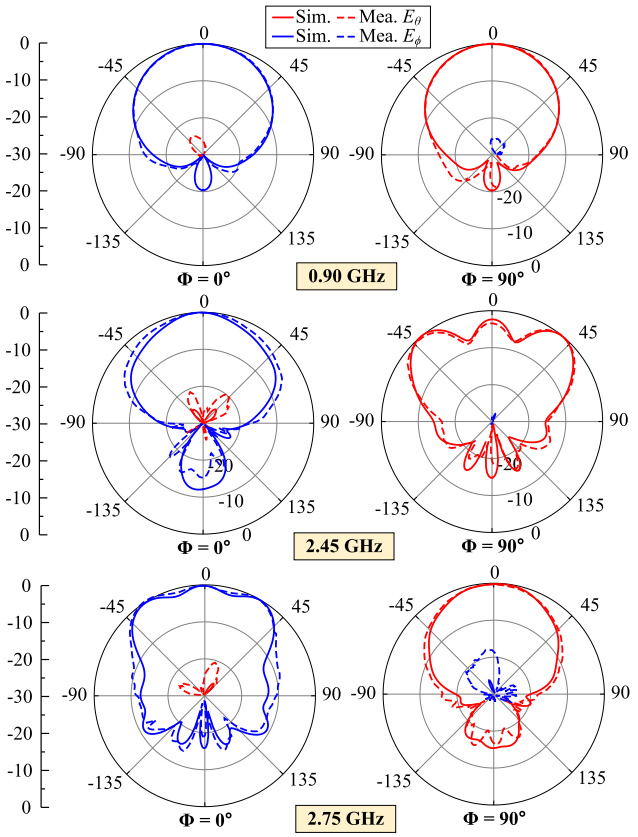

FIGURE 9. Normalized radiation pattern of the dual-band dual-LP antenna prototype when P2 is excited.

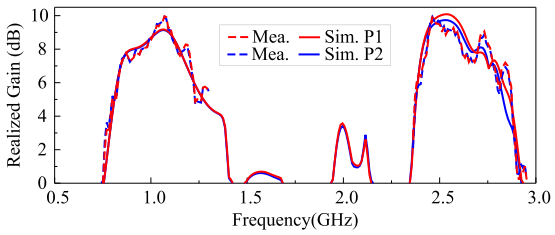

FIGURE 10. Realized gains of the dual-band dual-LP antenna prototype.

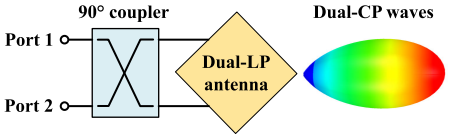

FIGURE 11. Schematic model of dual-CP antenna based on dual-LP radiating element and 90° hybrid coupler.

and thickness of 0.8128 mm). Its performances are mainly determined by the characteristic impedance and electric length of branch lines ($Z_{1,4}$ and $\theta_{1,4}$) and stubs ($Z_{2,3,5,6}$ and $\theta_{2,3,5,6}$). Following the analysis in [30], the 90° hybrid coupler is optimized for working at 0.9 and 2.45 GHz bands.

The dual-band 90° hybrid coupler is computationally characterized by using the ANSYS Electronics Desktop and its performances are given in Fig. 14. It is observed that the

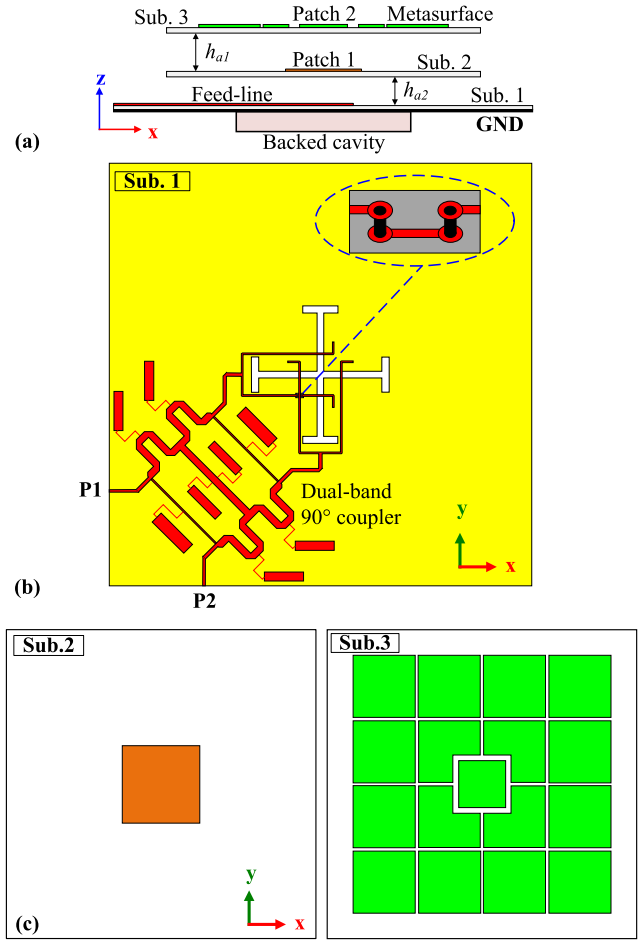

FIGURE 12. Geometry of the dual-band dual-CP antenna.

coupler achieves a good performance at the desired bands. The simulations result in reflection coefficients (e.g., S_{11}) and isolation (S_{41}) are < -15 dB at 0.86−1.18 GHz and 2.32−2.64 GHz. At these frequency ranges, S_{21} and S_{31} have a nearly equal magnitude (3.5±0.7 dB). S_{21} and S_{31} have a phase difference of 90° and −90° at the lower and upper bands, respectively. In contrast, S_{24} and S_{34} have a phase difference of −90° and 90° at the lower and upper bands, respectively.

C. FABRICATION AND MEASUREMENT

For verification, the dual-band dual-CP antenna has been fabricated and measured. Its prototype with overall size of $24 \times 24 \times 3.4$ cm^3 ($0.72\lambda \times 0.72\lambda \times 0.1\lambda$ at 0.9 GHz) is given in Fig. 15. Two 3.5-mm SMA connectors are employed as the microstripline-to-coaxial transformers. The measured and simulated results of the antenna prototype are given in Figs. 16, 17, 18, and 19 which indicate that the simulations agreed rather closely with the measurements.

From Fig. 16, the measurements result in an impedance-matching bandwidth of 0.81−1.17 and 2.30−2.60 GHz for 10-dB return loss and a port-to-port isolation ≥ 10 dB at 0.86−1.10 and 2.33−2.56 GHz. The measurements result

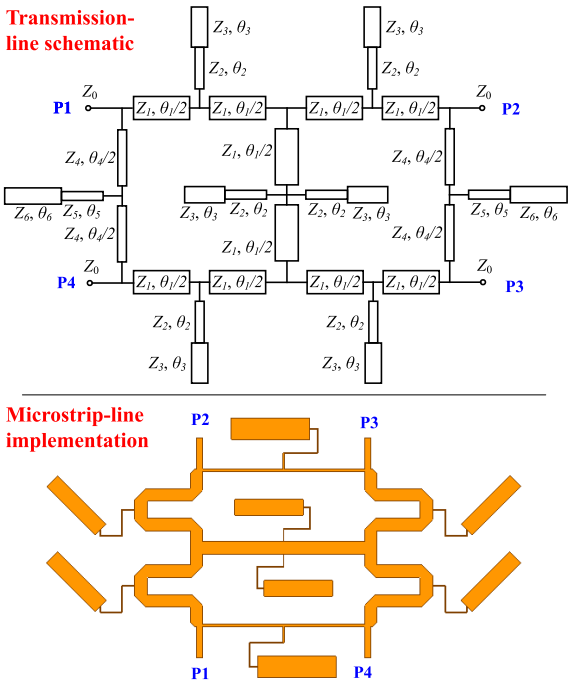

FIGURE 13. Transmission-line schematic and microstrip-line implementation of dual-band hybrid coupler. Its optimized parameters for 0.9 and 2.45 GHz are as: $Z_0 = 50\ \Omega$, $Z_1 = 29.68\ \Omega$, $\theta_1 = 81.78°$, $Z_2 = 136.09\ \Omega$, $\theta_2 = 34.83°$, $Z_3 = 24.96\ \Omega$, $\theta_3 = 40.34°$, $Z_4 = 80.36\ \Omega$, $\theta_4 = 89.11°$, $Z_5 = 119.41\ \Omega$, $\theta_5 = 42.79°$, $Z_6 = 18.98\ \Omega$, $\theta_6 = 46.45°$.

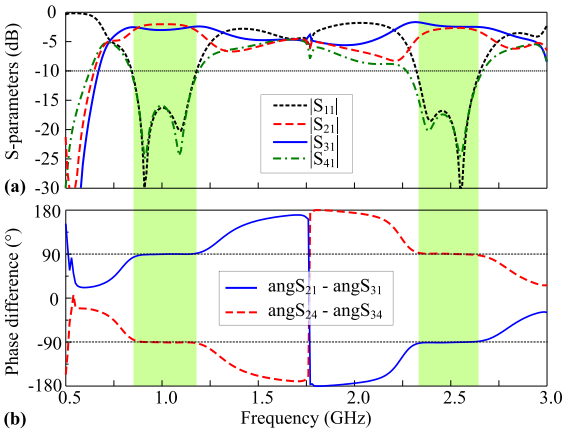

FIGURE 14. Simulated (a) S-parameters and (b) phase differences of the dual-band hybrid coupler.

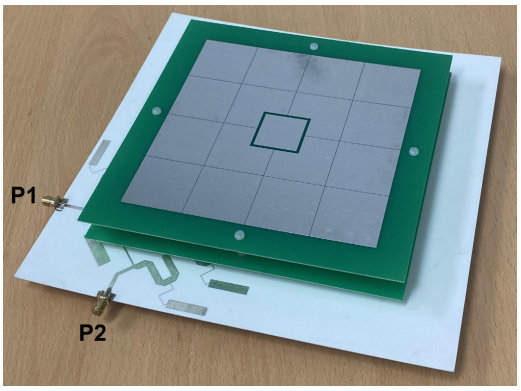

FIGURE 15. A fabricated prototype of the dual-band dual-CP antenna.

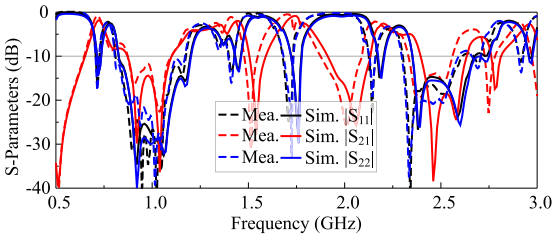

FIGURE 16. Simulated and measured S-parameters of the dual-band dual-CP antenna prototype.

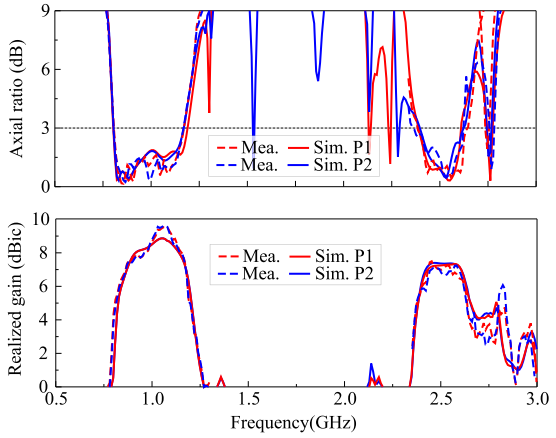

FIGURE 17. (a) axial ratio and (b) realized gain of the dual-band dual-CP antenna prototype.

in the peak isolation values of 23 and 26 dB for the lower and upper bands, respectively, which are smaller than the corresponding simulated values of 30 and 38 dB. This degradation is due to the imperfect structure of realized feeding network.

Fig. 17(a) shows the axial ratios of the dual-band dual-CP antenna prototype. For the both ports, the simulation and measurement result in axial ratio below 3 dB at 0.83−1.17 and 2.38−2.62 GHz. In addition, the measured axial ratios are less than 1.5 dB at the UHF and 2.45-GHz RFID bands. As shown in Fig. 17(b), the measured peak gains are 9.5 and 7.0 dBic at the lower and upper bands, respectively, which are relative to the corresponding simulated values of 8.9 and 7.3 dBic.

Figs. 18 and 19 illustrate the normalized radiation pattern of the dual-band dual-CP antenna prototype when P1 and P2 are excited, respectively. The measured patterns are shown to closely agree with the simulations. Both indicate that the proposed design achieves a good dual-sense CP radiation at the dual operation bands. For P1 excitation, the antenna yields left-hand CP (LHCP) at the lower band and right-hand CP (RHCP) at the upper band. For P2 excitation, it is RHCP

TABLE 2. A comparison of the dual-band antennas for UHF/ISM 2.45 GHz RFID readers.

Ant.	Structure	Overall size (λ_L)	10-dB RL BW (MHz)	3-dB AR BW (MHz)	Ports and Polarization	Gain (dB)	Radiation
[9]	Aperture coupled patch	0.22×0.48 × 0.048	812−1017 2360−2480	–	One port & single LP	1.5(L), 6.0(U)	Unidirectional
[10]	Slotted antenna	0.32×0.32 × 0.005	840−955 2400−2590	600−1200 1300−3000	One port & single CP	3.4(L), 5.4(U)	Quasi-omnidirectional
[11]	Stacked patches	0.33×0.33 × 0.02	903−938 2180−2590	911−933 2110−2640	One port & single CP	3.8(L), 8.9(U)	Unidirectional
[12]	Cross dipole	0.26×0.26 × 0.005	871−1279 2160−2800	882−936 2350−2580	One port & single CP	0.66(L), 2.6(U)	Bidirectional
[13]	Serial aperture-coupled patch	0.36×0.36 × 0.033	900−940 2320−2570	890−940 2220−2580	One port & single CP	3.8(L), 9.08(U)	Unidirectional
[14]	Aperture-coupled patch	0.45×0.45 × 0.031	840−980 1790−2740	901−941 2200−2730	One port & single CP	7.2(L), 8.2(U)	Unidirectional
[15]	Patch and AMC	0.64×0.64 × 0.09	903−927 2424−2472	902−950 2423−2470	One port & single CP	2.9(L), 6.05(U)	Unidirectional
[16]	Cross dipole and AMC	0.78×0.78 × 0.1	740−1100 2000−3000	770−1060 2230−2950	One port & dual CP	9.1(L), 15.2(U)	Unidirectional
[17]	Dipole-monopole and AMC	0.73×0.73 × 0.1	750−1100 2000−3000	820−1030 2250−2860	One port & dual CP	8.8(L), 13.3(U)	Unidirectional
[21]	Aperture-coupled patch	0.76×0.76 × 0.07	860−940	860−940	Two port & dual CP	6.0(L)	Unidirectional
[22]	Aperture-coupled patch	0.66×0.66 × 0.1	850−1000 2250−2600	870−990 2380−2580	Two port & dual CP	6.6(L), 7.9 (U)	Unidirectional
Prop. LP	Aperture-coupled patch	0.72×0.72 × 0.1	860−1080 2400−2750	–	Two port & dual LP	10(L), 9.3(U)	Unidirectional
Prop. CP	Aperture-coupled patch	0.72×0.72 × 0.1	810−1170 2300−2600	830−1170 2380−2620	Two port & dual CP	9.5(L), 7.0(U)	Unidirectional

λ_L is the free-space wavelength referring to 900 MHz; AMC: artificial magnetic conductor; RL BW: return-loss bandwidth; AR BW: axial ratio bandwidth; L: lower band; U: upper band.

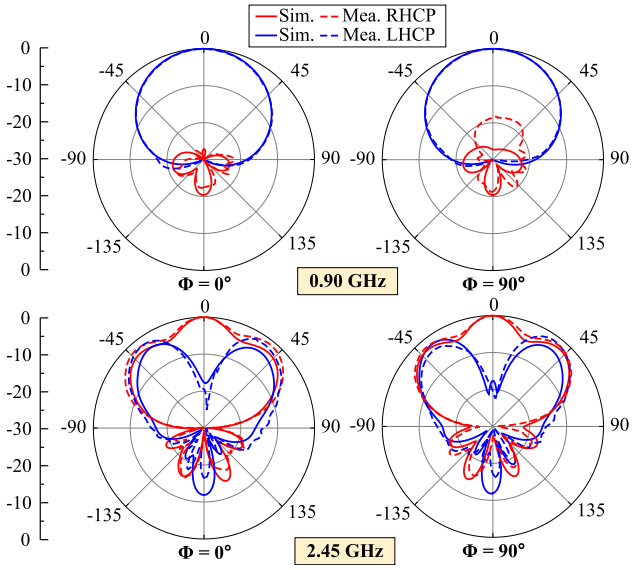

FIGURE 18. Normalized radiation pattern of the dual-band dual-CP antenna prototype when P1 is excited.

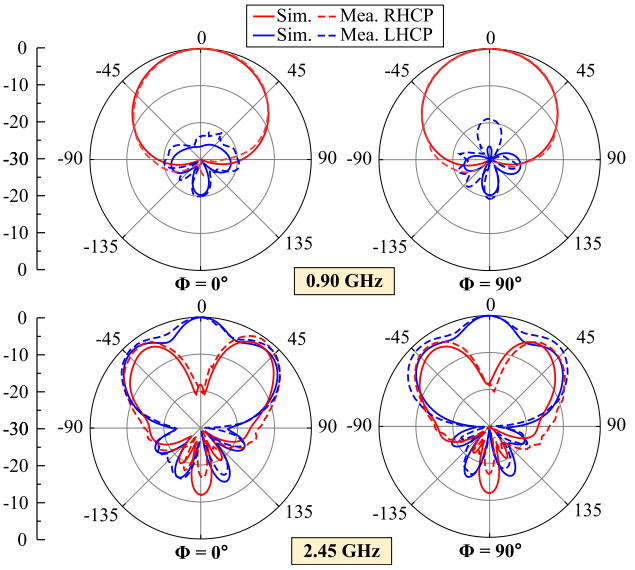

FIGURE 19. Normalized radiation pattern of the dual-band dual-CP antenna prototype when P2 is excited.

for the lower band and LHCP for the upper band. Similar to the LP antenna, the higher-order mode of the metasurface alo affects the dual-CP radiation at the upper band; i.e., at 2.45 GHz, the antenna prototype yields a narrow 3-dB AR beamwidth of $\sim 20°$. Moreover, for both bands, the prototype shows a highly symmetric pattern and a cross-polarization level ≤ -18 dB at the broadside direction. In the $\Phi = 0°$ and $\Phi = 90°$ planes, the HPBWs are $67° \pm 3°$ and $50° \pm 5°$ at 0.9 and 2.45-GHz, respectively.

IV. COMPARISON AND DISCUSSION

Table 2 shows a comprehensive comparison between the dual-band antennas for UHF/ISM 2.45 GHz RFID readers. For the handheld RFID readers, the designs in [9], [10], [11], and [12] have compact-size and lightweight, but suffer a

low gain which restricts the readable range. The operational bandwidths of antennas in [13], [14], and [15] do not completely cover the UHF/ISM-2.45 GHz RFID bands. As compared with these antennas, our designs yield a wider bandwdith and higher gain. Although the sequentially rotated arrays in [16] and [17] achieved dual wideband, high gain, and dual CP radiation, which are with a single input port, and consequently, not very preferred for the compact RFID MIMO systems. The two-port design in [21] operates at the UHF band only, while the dual-band dual-CP antenna [22] suffers a narrow band for 10-dB isolation bandwidth. Relative to [22], the proposed antennas yield a comparable size, but significantly wider bandwidth, higher gain, and higher isolation. As a result, the proposed antennas with two input ports yield dual wideband, high gain, and high port-to-port isolation. The dual wideband makes the proposed antennas suitable for a universal UHF/ISM 2.45 GHz RFID reader. The high gain allows a long communication distance between the readers and tags. The high port-to-port isolation could improve the RFID sensitivity.

V. CONCLUSION

We have presented dual-band dual LP/CP antennas for the UHF and 2.45GHz RFID readers. The antennas employ a metasurface and two stacked patches as the primary radiating elements; i.e., the metasurface is for the UHF band, while the patches are for the 2.45 GHz band. The radiating elements are fed by a feeding structure composed of two orthogonal microstrip lines and a crossed slot to produce the dual-band dual-LP radiation. For reducing the back radiation from the cross slot, the antenna is backed by a metallic cavity. In order to generate the dual-band dual-CP radiation, the dual-LP antenna is incorporated with a dual-band branch-line hybrid coupler. The fabricated antenna prototypes not only achieve impedance and 3-dB AR bandwidths completely covering the UHF ($860 - 960$ MHz) and ISM-2.45 GHz ($2400 - 2500$ MHz) bands but also yield good broadside radiation with stable pattern, high gain, low cross polarization, and high front-to-back ratio. In addition, both LP/CP designs yield high port-to-port isolation. These advantages make the proposed antennas to be a good candidate for dual-band RFID MIMO systems. Moreover, with the features of low profile, dual wideband, high isolation, and high efficiency, the proposed dual-LP antenna can be widely applied to next-generation mobile communication systems.

REFERENCES

[1] R. Want, "An introduction to RFID technology," *IEEE Pervasive Comput.*, vol. 5, no. 1, pp. 25–33, Jan./Mar. 2006.

[2] L. D. Xu, W. He, and S. Li, "Internet of Things in industries: A survey," *IEEE Trans. Ind. Informat.*, vol. 10, no. 4, pp. 2233–2243, Nov. 2014.

[3] H.-T. Hsu and T.-J. Huang, "A koch-shaped log-periodic dipole array (LPDA) antenna for universal Ultra-High-Frequency (UHF) radio frequency identification (RFID) handheld reader," *IEEE Trans. Antennas Propag.*, vol. 61, no. 9, pp. 4852–4856, Sep. 2013.

[4] X. Liu, Y. Liu, and M. M. Tentzeris, "A novel circularly polarized antenna with coin-shaped patches and a ring-shaped strip for worldwide UHF RFID applications," *IEEE Antennas Wireless Propag. Lett.*, vol. 14, pp. 707–710, 2015.

[5] C.-Y.-D. Sim, Y.-W. Hsu, and G. Yang, "Slits loaded circularly polarized universal UHF RFID reader antenna," *IEEE Antennas Wireless Propag. Lett.*, vol. 14, pp. 827–830, 2015.

[6] J. Li, H. Liu, S. Zhang, M. Luo, Y. Zhang, and S. He, "A wideband single-fed, circularly-polarized patch antenna with enhanced axial ratio bandwidth for UHF RFID reader applications," *IEEE Access*, vol. 6, pp. 55883–55892, 2018.

[7] R. Cao and S.-C. Yu, "Wideband compact CPW-fed circularly polarized antenna for universal UHF RFID reader," *IEEE Trans. Antennas Propag.*, vol. 63, no. 9, pp. 4148–4151, Sep. 2015.

[8] Q. Liu, J. Shen, H. Liu, Y. Wu, M. Su, and Y. Liu, "Low-cost compact circularly polarized directional antenna for universal UHF RFID handheld reader applications," *IEEE Antennas Wireless Propag. Lett.*, vol. 14, pp. 1326–1329, 2015.

[9] H.-T. Hsu and T.-J. Huang, "A 1×2 dual-band antenna array for radio-frequency identification (RFID) handheld reader applications," *IEEE Trans. Antennas Propag.*, vol. 62, no. 10, pp. 5260–5267, Oct. 2014.

[10] S. Kibria, M. T. Islam, and B. Yatim, "New compact dual-band circularly polarized universal RFID reader antenna using ramped convergence particle swarm optimization," *IEEE Trans. Antennas Propag.*, vol. 62, no. 5, pp. 2795–2801, May 2014.

[11] Q. Liu, J. Shen, J. Yin, H. Liu, and Y. Liu, "Compact 0.92/2.45-GH dual-band directional circularly polarized microstrip antenna for handheld RFID reader applications," *IEEE Trans. Antennas Propag.*, vol. 63, no. 9, pp. 3849–3856, Sep. 2015.

[12] F.-P. Lai, J.-F. Yang, and Y.-S. Chen, "Compact dual-band circularly polarized antenna using double cross dipoles for RFID handheld readers," *IEEE Antennas Wireless Propag. Lett.*, vol. 19, pp. 1429–1433, 2020.

[13] T.-N. Chang and J.-M. Lin, "Serial aperture-coupled dual band circularly polarized antenna," *IEEE Trans. Antennas Propag.*, vol. 59, no. 6, pp. 2419–2423, Jun. 2011.

[14] Q. Liu, J. Shen, H. Liu, and Y. Liu, "Dual-band circularly-polarized unidirectional patch antenna for RFID reader applications," *IEEE Trans. Antennas Propag.*, vol. 62, no. 12, pp. 6428–6434, Dec. 2014.

[15] S. Sarkar and B. Gupta, "A dual-band circularly polarized antenna with a dual-band AMC reflector for RFID readers," *IEEE Antennas Wireless Propag. Lett.*, vol. 19, pp. 796–800, 2020.

[16] R. Xu, J. Liu, K. Wei, W. Hu, Z.-J. Xing, J.-Y. Li, and S. S. Gao, "Dual-band circularly polarized antenna with two pairs of crossed-dipoles for RFID reader," *IEEE Trans. Antennas Propag.*, vol. 69, no. 12, pp. 8194–8203, Dec. 2021.

[17] R. Xu and Z. Shen, "Dual-band circularly polarized RFID reader antenna with combined dipole and monopoles," *IEEE Trans. Antennas Propag.*, vol. 71, no. 12, pp. 9593–9600, Dec. 2023.

[18] J. D. Griffin and G. D. Durgin, "Gains for RF tags using multiple antennas," *IEEE Trans. Antennas Propag.*, vol. 56, no. 2, pp. 563–570, Feb. 2008.

[19] S. Chen, S. Zhong, S. Yang, and X. Wang, "A multiantenna RFID reader with blind adaptive beamforming," *IEEE Internet Things J.*, vol. 3, no. 6, pp. 986–996, Dec. 2016.

[20] S. Haddadian, J. C. Scheytt, G. vom Bögel, and T. Grenter, "A sub-threshold microwave RFID tag chip, compatible with RFID MIMO reader technology," *IEEE J. Radio Freq. Identificat.*, vol. 7, pp. 556–563, 2023.

[21] X.-Z. Lai, Z.-M. Xie, Q.-Q. Xie, and X.-L. Cen, "A dual circularly polarized RFID reader antenna with wideband isolation," *IEEE Antennas Wireless Propag. Lett.*, vol. 12, pp. 1630–1633, 2013.

[22] Y.-K. Jung and B. Lee, "Dual-band circularly polarized microstrip RFID reader antenna using metamaterial branch-line coupler," *IEEE Trans. Antennas Propag.*, vol. 60, no. 2, pp. 786–791, Feb. 2012.

[23] C. H. Tsao, Y. M. Hwang, F. Kilburg, and F. Dietrich, "Aperture-coupled patch antennas with wide-bandwidth and dual-polarization capabilities," in *Proc. IEEE AP-S Int. Symp., Antennas Propag.*, vol. 3, Jun. 1988, pp. 936–939.

[24] I. Nystrom and D. Karlsson, "Reduction of back radiation and cross-coupling in dual polarized aperture coupled patch antennas," in *Proc. IEEE Antennas Propag. Soc. Int. Symp. Dig.*, vol. 4, Jul. 1997, pp. 2222–2225.

[25] J. Wang, Y. Li, Z. H. Jiang, T. Shi, M.-C. Tang, Z. Zhou, Z. N. Chen, and C.-W. Qiu, "Metantenna: When metasurface meets antenna again," *IEEE Trans. Antennas Propag.*, vol. 68, no. 3, pp. 1332–1347, Mar. 2020.

[26] F. Costa, O. Luukkonen, C. R. Simovski, A. Monorchio, S. A. Tretyakov, and P. M. de Maagt, "TE surface wave resonances on high-impedance surface based antennas: Analysis and modeling," *IEEE Trans. Antennas Propag.*, vol. 59, no. 10, pp. 3588–3596, Oct. 2011.

[27] S. X. Ta and I. Park, "Artificial magnetic conductor-based circularly polarized crossed-dipole antennas: 2. AMC structure without grounding pins," *Radio Sci.*, vol. 52, no. 5, pp. 642–652, May 2017, doi: 10.1002/2016RS006204.
[28] S. X. Ta, N. Nguyen-Trong, V. C. Nguyen, K. K. Nguyen, and C. Dao-Ngoc, "Broadband dual-polarized antenna using metasurface for full-duplex applications," *IEEE Antennas Wireless Propag. Lett.*, vol. 20, pp. 254–258, 2021.
[29] S. X. Ta, V. C. Nguyen, B.-T. Nguyen-Thi, T. B. Hoang, A. N. Nguyen, K. K. Nguyen, and C. Dao-Ngoc, "Wideband dual-circularly polarized antennas using aperture-coupled stacked patches and single-section hybrid coupler," *IEEE Access*, vol. 10, pp. 21883–21891, 2022.
[30] K.-S. Chin, K.-M. Lin, Y.-H. Wei, T.-H. Tseng, and Y.-J. Yang, "Compact dual-band branch-line and rat-race couplers with stepped-impedance-stub lines," *IEEE Trans. Microw. Theory Techn.*, vol. 58, no. 5, pp. 1213–1221, May 2010.

THI NGOC HIEN DOAN received the degree in telecommunication engineering, the master's degree in information processing, communication, and the Ph.D. degree from the School of and Telecommunication (SET), Hanoi University of Science and Technology, Vietnam (HUST), in 2002, 2005, and 2020, respectively. From 2003 to 2021, she works as a Researcher at the International Research Institute of Multimedia Information, Communication and Applications (MICA), HUST. Since 2021, she has been a Lecturer with the School of Electrical and Electronics (SEEE), HUST, and a Researcher with CRD Lab, HUST. Her research interests include microstrip antennas, RFID antennas, and antennas for SAR.

KHAC KIEM NGUYEN (Member, IEEE) was born in Hanoi, Vietnam, in 1978. He received the B.Eng., M.Sc., and Ph.D. degrees from the School of Electronics and Telecommunication (SET) (now renamed as the School of Electrical and Electronic Engineering (SEEE), Hanoi University of Science and Technology (HUST), Vietnam, in 2001, 2003, and 2017, respectively. Since 2001, he has been a Lecturer with SEEE, HUST, and a Researcher with CRD Lab, HUST. His research interest includes design microstrip antenna for next generation mobile communication systems as well as passive RF components.

SON XUAT TA (Senior Member, IEEE) received the B.Sc. (Eng.) degree in electronics and telecommunications from Hanoi University of Science and Technology, Vietnam, in August 2008, and the Ph.D. degree in electrical engineering from Ajou University, South Korea, in February 2016. From March 2016 to February 2017, he was a Postdoctoral Research Fellow at the Department of Electrical and Computer Engineering, Ajou University. From March 2017 to August 2017, he was at the Division of Computational Physics, Institute for Computational Science, and the Faculty of Electrical and Electronics Engineering, Ton Duc Thang University, Ho Chi Minh City, Vietnam. Since 2017, he has been a Lecturer with the School of Electronics and Telecommunication (now renamed as School of Electrical and Electronic Engineering), Hanoi University of Science and Technology. He has authored or co authored more than 100 technical journals and conference papers. His research interests include antennas, metamaterials, metasurfaces, metamaterial-based antennas, metasurface-inspired antennas, circularly polarized antennas, and millimeter-wave antennas. He served as a reviewer for more than 15 scientific journals. He has been selected as a Top Reviewer for IEEE TRANSACTIONS ON ANTENNAS AND PROPAGATION in 2020–2023.